Pergamon

Journal of Structural Geology, Vol. 16, No. 10, pp. 1431 to 1446, 1994

0191-8141/94 $7.00+0.00

0191-8141(94)E0004-I

Preferred crystallographic orientation development during the plastic and superplastic flow of calcite rocks

E. H. RUTTER

Department of Geology, Rock Deformation Laboratory, University of Manchester, Manchester M13 9PL, U.K.

M. CASEY

Geologisches Institut, ETH-Zentrum, CH-8092, Zürich, Switzerland

and

L. BURLINI

Dipartimento Scienze Terra, via Botticelli 23, Universita di Milano, 20133 Milano, Italy

(*Received* 5 *August* 1993; *accepted in revised form* 20 *December* 1993)

Abstract—Grain-size sensitive flow of fine-grained rocks, such as are often found in mylonitic shear zones, is commonly inferred to be accomplished by grain-boundary sliding, so that no preferred crystallographic orientation is expected to develop, pre-existing fabrics are supposed to weaken and grain shapes to remain equant. However, many fine-grained mylonites commonly exhibit marked preferred crystallographic orientation, whilst displaying a stable but weak grain-shape fabric.

We have examined preferred crystallographic orientation and shape fabric development during the flow of synthetic, ultrafine-grained (<10 μm), hot-pressed calcite rocks, Solnhofen limestone and Carrara marble. Samples were deformed experimentally both in extension and compression, under conditions encompassing the transition from grain-size insensitive crystal-plastic flow to grain-size sensitive superplastic flow (300–>700°C).

The strong crystal-plastic fabric develops more slowly but is not eliminated through the broad transition into true superplastic flow. This is interpreted to reflect an important role of intracrystalline plasticity in the accommodation of grain-boundary sliding.

From experiments designed to investigate the extent of survival or modification of an initial twinning fabric through recrystallization and subsequent hot working, it was shown that although the microstructure could be totally annealed, the early formed fabric survived even subsequent high-temperature crystal-plastic or superplastic flow. This may explain the frequent occurrence of strong, low-temperature fabrics in calcite ultramylonites.

INTRODUCTION

PLASTIC (i.e. non-cataclastic) shear zones in rocks are generally characterized by intense grain-size reduction. An accompanying equigranular microstructure which appears insensitive to the amount of strain has commonly led geologists to surmise that the deformation was dominated by high-temperature grain-boundary sliding (superplastic flow) (e.g. Boullier & Gueguen 1975, Schmid *et al.* 1977, Behrmann & Mainprice 1987). On the basis of observations made on superplastic engineering materials (e.g. Padmanabhan & Lücke 1986, Bowen & Hirsch 1988) it is widely held that large-strain flow dominated by grain-boundary sliding and rotation should be characterized by a lack of a strong crystallographic preferred orientation (CPO). On the other hand, many grain-refined mylonites display quite strong crystallographic fabrics together with an equigranular shape fabric, and this has led some to infer that the flow was dominated by crystal-plastic deformation accompanied by cyclic dynamic recrystallization (e.g. White 1976, Tullis & Yund 1985). For example, Fig. 1 shows the strong CPO of a natural calcite mylonite and Fig. 2(a) the corresponding fine-grained, almost equigranular microstructure. Not only is this fabric strong, but it is of the type normally associated with low temperature plasticity involving deformation twinning, yet the microstructure shows no sign of twinning activity. These are common characteristics of calcite mylonites from a variety of localities.

Little information is available from experiments on rocks regarding crystallographic preferred orientation development during superplastic flow. Schmid *et al.* (1977) and Casey *et al.* (1978) showed that during the superplastic flow of Solnhofen limestone only a weak CPO developed, at least up to shortening strains of *ca* 30%. For other rock types, much less information is available. Here we investigate the crystallographic fabric transition from intracrystalline-plastic to superplastic flow in the deformation of fine-grained calcite rocks. For the most part, these new experiments have been carried out on synthetic aggregates hot-pressed from the same

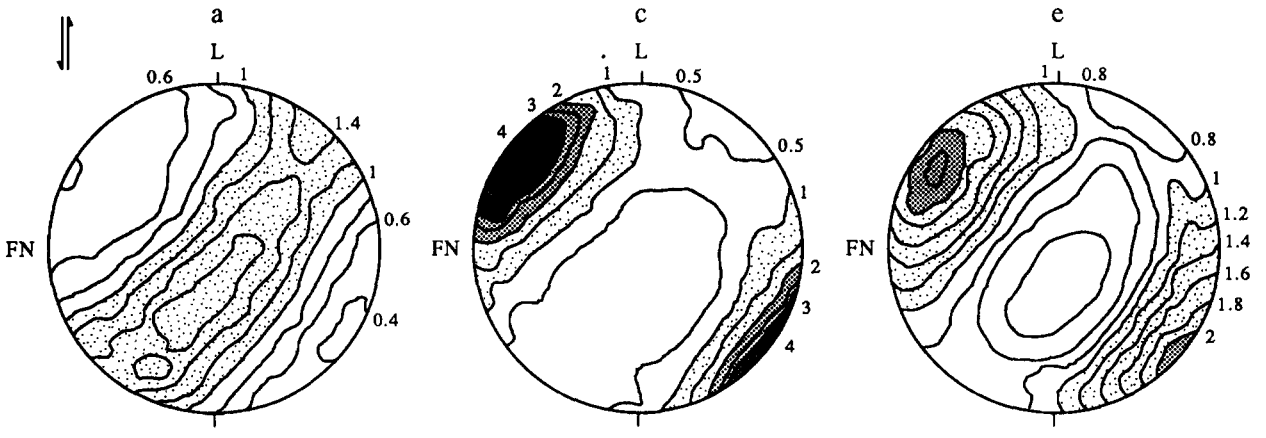

Fig. 1. Crystallographic preferred orientation of calcite ultramylonite from the root zone of the Morcles nappe (location, Saillon quarry), Switzerland. L indicates lineation direction and FN the foliation normal. The fabric shows a maximum normal to the *e* twin plane, oblique to the foliation plane. This is the fabric type normally associated with relatively low-temperature deformation involving *r* glide and deformation twinning. Contours are in multiples of a uniform distribution (indicated). This fabric was described by Schmid *et al.* (1981).

powder batches as used in our previous study on synthetic calcite rocks (Walker *et al.* 1990), and we correlate superplastic flow with the regimes of grain-size sensitive flow mapped out in the previous study. It was shown that the grain-size sensitive flow involved grain-boundary sliding accommodated by a mixture of diffusion and intracrystalline plasticity.

In this paper we address the following specific questions by means of high-temperature–pressure experiments, followed by preferred orientation studies.

(a) What is the starting CPO of synthetic, hot-pressed calcite rocks?

(b) What is the evolution of fabric type through the plastic–superplastic transition and what is the rate of change of fabric intensity with strain?

(c) How do these factors compare for uniaxial compression and extension strain paths?

(d) Do CPOs produced during working by intracrystalline plastic flow survive recrystallization and grain growth, and are they modified by subsequent coaxial redeformation in a different deformation mechanism field?

STARTING MATERIALS

For most of the experiments described here, synthetic, pure calcite rocks of controlled ultrafine grain size were prepared by hot, isostatic pressing (HIP). Powders were prepared by crushing and grinding clear, Iceland spar crystals. The fraction less than 64 μm was extracted by sieving, then several finer size fractions were separated by successively centrifuging suspensions in water as described by Walker *et al.* (1990). Powders of mean size 3.5, 7.5 and 38 μm were used to fabricate the cylindrical (9.5 mm diameter × 20 mm long) specimens for deformation. After HIP (3 h at 550°C followed by 1 h at 700°C, in each case at 200 MPa confining pressure), the maximum porosity of the samples was 3%, and the microstructure was an equigranular foam texture, with straight or gently curving grain boundaries and free from twins (Fig. 2b).

Following our previous procedures (Walker *et al.* 1990), some of the cylinders were prepared first by uniaxial cold-pressing the powder into 0.25 mm wall-thickness copper tubes in a die at a nominal 600 MPa. This cold-pressing technique produces a high degree of initial compaction (a high green density), which minimizes the further compaction that occurs during the HIP stage. However, it seemed likely that some considerable deviatoric stress would be induced during the cold pressing, with the attendant possibility that a low-temperature crystallographic fabric might be induced in the starting material. For this reason most of the new samples were fabricated by truly isostatic hot-pressing, without an initial cold uniaxial pressing stage. This resulted in slightly smaller sample diameters of the densified cylinders. We have studied the preferred orientation developed in specimens prepared using both techniques.

In addition to experiments on synthetic samples prepared as described above, we have also run deformation experiments on 9.5 mm diameter cylinders of Solnhofen limestone (4 μm grain-size) for comparison. The block from which the samples were cored was that used by Rutter (1974). Its microstructures and mechanical behaviour is virtually identical to samples deformed by Schmid *et al.* (1977). Compared to the pure, synthetic calcite aggregates, Solnhofen limestone is slightly stronger and contains up to 4% of impurity phases in the grain boundaries. These impurities are powerful inhibitors of grain growth at high temperatures (Olgaard & Evans 1986, Covey-Crump & Rutter 1989, Walker *et al.* 1990).

Over most of the experimental conditions to which the fine-grained samples were subjected, deformation takes place in regimes of grain-size sensitive flow. In order to compare the fabrics produced with those characteristic of the grain-size insensitive flow of coarser-grained rocks, some experiments have been run on Carrara Marble (mean grain size about 130 μm).

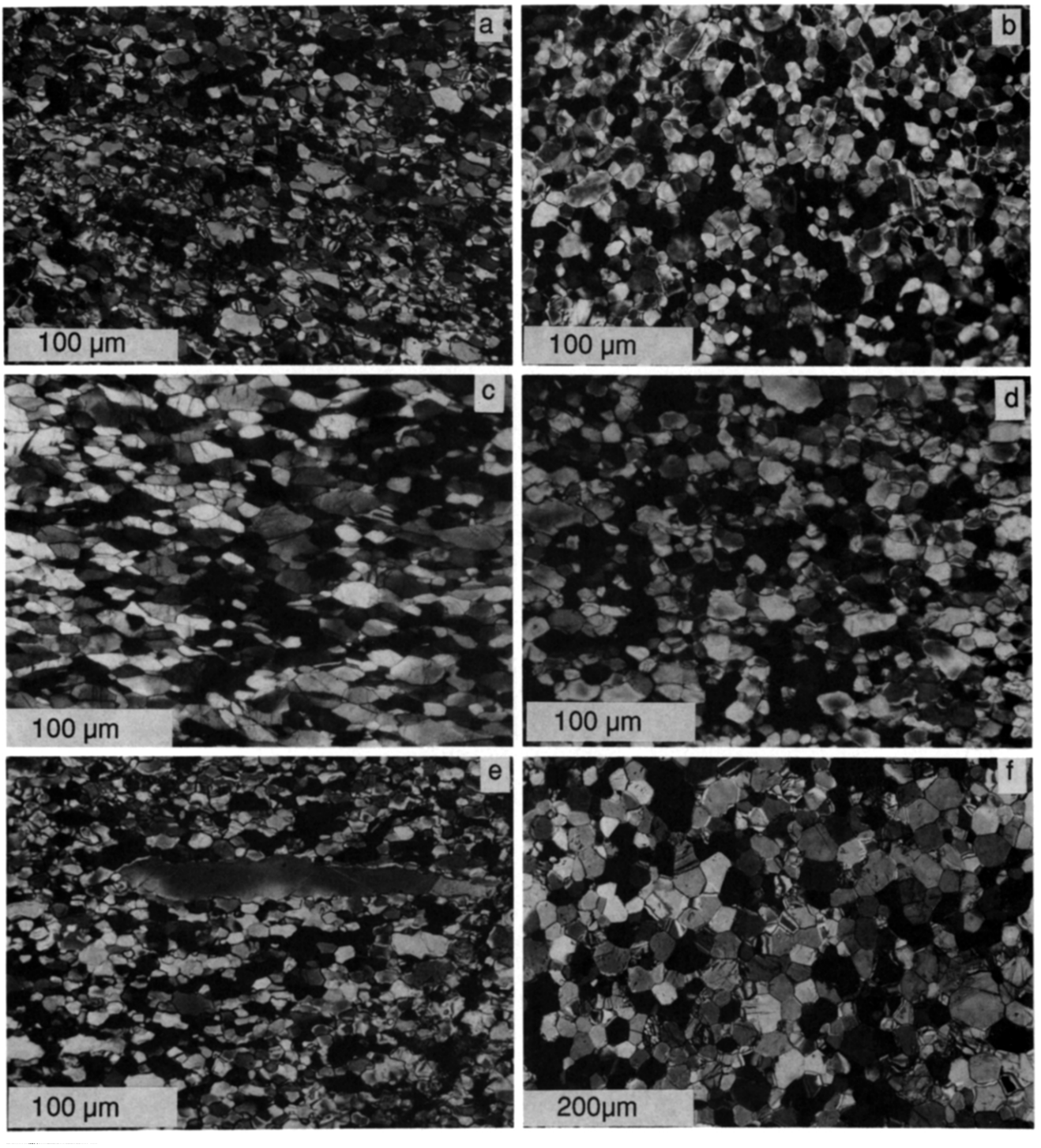

Fig. 2. Optical micrographs, all crossed polars. For experimentally deformed samples the relative compression direction is parallel to the short side of the micrograph. (a) Microstructure of a high-strain calcite mylonite (from the same locality) whose CPO is identical to that shown in Fig. 1. Grain size is 6.3 ± 1.5 μm, reduced from protolith of *ca* 100 μm. The grains show a weak shape fabric (1:1.62) parallel to the macroscopic foliation defined by streaks of colour variation. Section is cut normal to foliation and parallel to lineation, which is in turn parallel to the long side of the photograph. (b) An ultrathin section of synthetic calcite rock after hot isostatic pressing (specimen L14). Grains are equidimensional, possess straight or gently curving boundaries and are free from twinning. (c) Optical microstructure of sample L4, shortened 30% in the regime of twinning-absent intracrystalline plastic flow. There is a marked grain shape fabric and few grains contain twins. (d) & (e) respectively; sample L24, at points corresponding to the positions along the sample for which CPOs are shown in Fig. 11. At low strains the microstructure is isotropic equigranular, whereas a weak, steady-state shape fabric has developed at high strain. In (e) an embedded large grain has deformed by intracrystalline plasticity, its shape tracking the bulk strain, in contrast to the behaviour of the finer grains. (f) Equigranular microstructure produced during flow to 30% strain in the low-stress, grain-size sensitive regime, in synthetic sample L30.

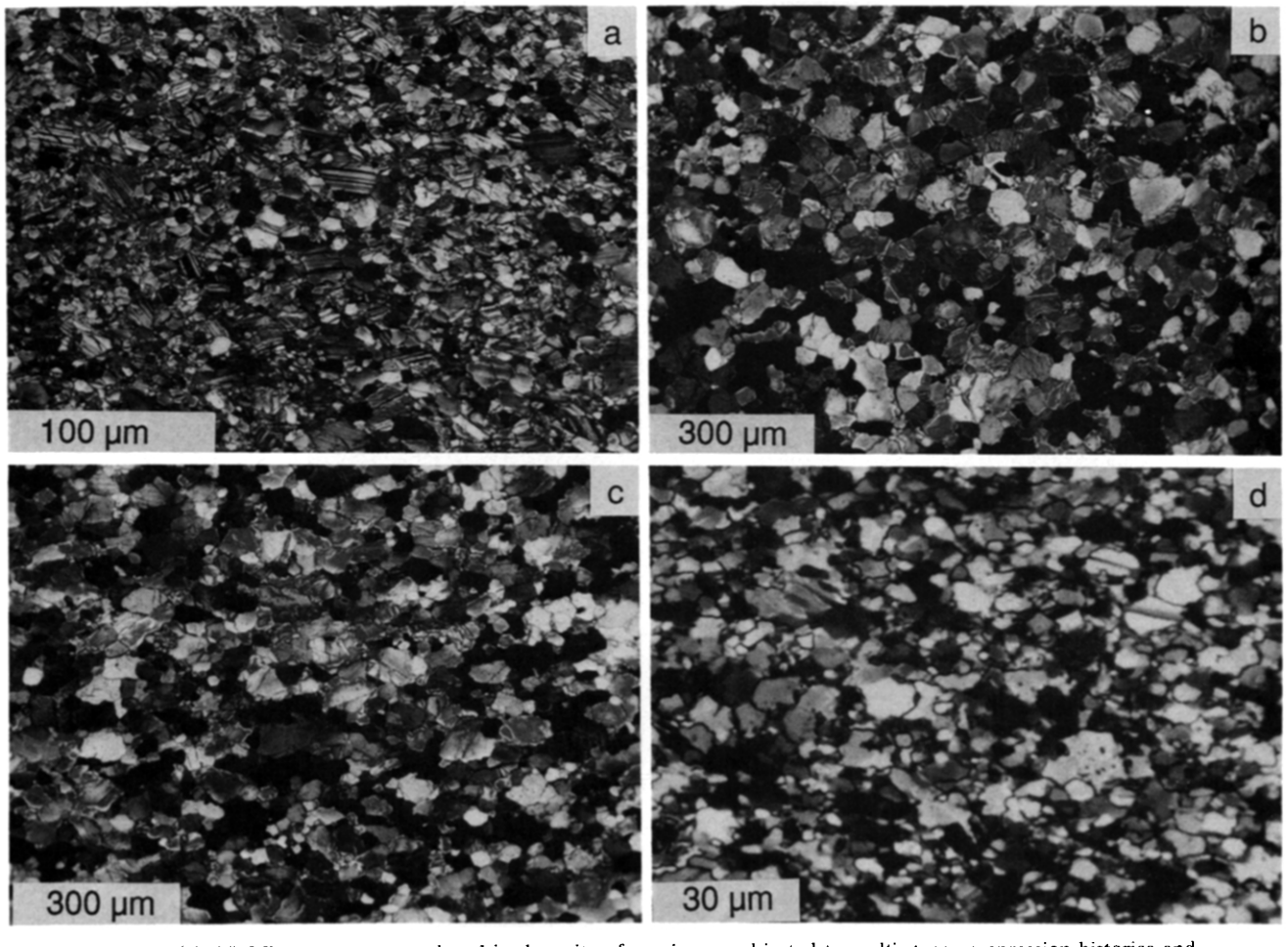

Fig. 3. (a)–(d) Microstructures produced in the suite of specimens subjected to multi-stage compression histories and whose CPOs are illustrated in Fig. 14. (a) The distinct shape fabric and marked degree of twinning activity in the initially cold worked (12% shortening) sample L34. (b) The isotropic shape fabric and grain growth resulting from annealing at 700°C following the initial cold working. Twins have been removed by twin boundary migration recrystallization (specimen L35). (c) Slight shape fabric, grain growth and lack of twinning in sample L36 reworked in the high-stress, grain-size sensitive flow field. (d) Weak residual shape fabric, no significant grain growth and lack of twinning in sample So15 reworked in the low-stress, grain-size sensitive flow field.

EXPERIMENTAL METHODS

(a) Heat treatment and deformation runs

All hot-pressing and deformation runs were carried out with the cylindrical specimen mounted between axial loading pistons and inside 0.25 mm wall-thickness annealed copper jackets. Specimens were kept in an oven at 100°C prior to use. In all cases the usual rock mechanics technique of venting the specimen pores to atmosphere via an axial hole in one of the loading pistons was not used owing to the tendency for the weak rock to be extruded through such a hole. The effects of a substantial leak of confining pressure fluid into the sample can usually be detected from anomalous mechanical behaviour.

Two types of fluid-medium deformation machine have been used. For temperatures up to 700°C, an externally heated NIMONIC (75% nickel) alloy vessel (Rutter *et al.* 1985) was used, with water as the confining medium. NIMONIC alloy spacers were placed between the loading pistons and the specimen ends. For some runs at 700°C and all higher temperature runs an internally-heated Paterson Instruments gas-medium machine was used. At 700°C copper jackets alone could be employed, but at 800 and 900°C a short copper sleeve was in contact with the specimen. Isolation from the confining medium at these higher temperatures required an outer iron jacket to be used. At such temperatures a long copper jacket conducts too much heat away from the furnace hot-spot.

In both machines, specimens could be deformed either in compression or in extension. Extension testing of rocks at high temperatures is not new. It was favoured by H.C. Heard in particular (e.g. Heard & Raleigh 1972), but its potential in rock mechanics has never been fully realized. The advantages of extensional testing under confining pressure to large strains as currently employed in our laboratory will form the subject of further publications. For the present purposes, however, it will suffice to note that it allows an alternative strain pathway to be used for preferred orientation studies. It also allows enormous strains to be accessed if a necking instability develops, whilst allowing those strains to be accurately measured from the local fractional reduction of cross-sectional area of the sample. Large strain testing (>30% shortening) in compression is limited by the development of extremely heterogeneous deformation (and microstructures) as the specimen flows around the ends of the loading pistons. In the gas apparatus at large shortenings (much above 20%) buckling of the specimen tends to develop because lateral restraints cannot be applied to the long axial column by the relatively delicate internal furnace. In contrast, even at large strains in extension the deformation remains truly axial, and the deformation of short sections of the specimen along its axis can be considered homogeneous. Because each section of the specimen normal to the extension direction must support the same force, at the end of the test the stress across every cross-section of the specimen normal to the axis can be accurately determined. This is not true for compressed samples, because the stress is not homogeneous within a given cross-section normal to the unique axis.

All compression tests reported here were carried out at 200 MPa confining pressure and extension tests at either 250, 300 or 350 MPa confining pressure. Thus the mean pressure during the flow of all samples was less disparate than if all tests were carried out at the same applied confining pressure. In all cases reported temperatures are believed accurate to within ±5°C of the stated value, and temperature variation along the length of samples did not exceed 10°C. Differential loads in the Nimonic apparatus were measured using a semi-internal (free of the effects of moving seal friction but pressure-sensitive) load cell of the Heard (1963) type. In the gas apparatus differential load was measured using a fully-internal capacitance load cell marketed by Paterson Instruments Pty. Both load cells can resolve loads corresponding to less than 1 MPa on the sample, but hysteresis on the zero-load position meant that this is the practical level of reproducibility on load measurements.

All deformation tests were carried out at constant displacement rate, corresponding to strain-rates in the range 10^{-4}–10^{-7} s^{-1}. The lower strain-rates were used only when it was desired to access conditions favouring a particular deformation mechanism. Generally, at the end of a test the temperature was lowered as rapidly as possible, to minimize static changes to the microstructure (e.g. grain shape and size). In the gas-medium machine, temperature falls 150°C from 700°C in the first minute, whereas in the Nimonic machine the cooling rate is 10 times slower.

(b) Microstructural and textural studies

The inverse pole figures for experimentally deformed material were calculated from X-ray scans obtained from a Scintag XDS2000 texture goniometer. Thin sections of around 120 μm thick were prepared from the experimentally deformed material. The section was cut so that the symmetry axis of each deformed specimen lay in the plane of the section. The sections were fixed to their glass slides using histological wax so that they could be removed by melting, and then mounted on a tape of low X-ray absorbance. The presence of a symmetry axis in the specimen means that the preferred orientation of a given crystal plane can be represented as a profile scan taken from parallel to the symmetry axis to an angle 90° to it. In the present study the specimens were scanned in transmission mode. Two complete rotations of the specimen were measured, one with zero tilt and one with 1° tilt. The use of this procedure was determined by the measurement software of the goniometer. Data from the eight quadrants thus measured were averaged into one quadrant. For coarse-grained Cararra marble specimens, measurements from four separate areas of the specimen were taken and averaged. The diffraction peaks 012 (*f*), 104 (*r*), 006 (*c*), 110 (*a*), 113, 202 (*h*), 018

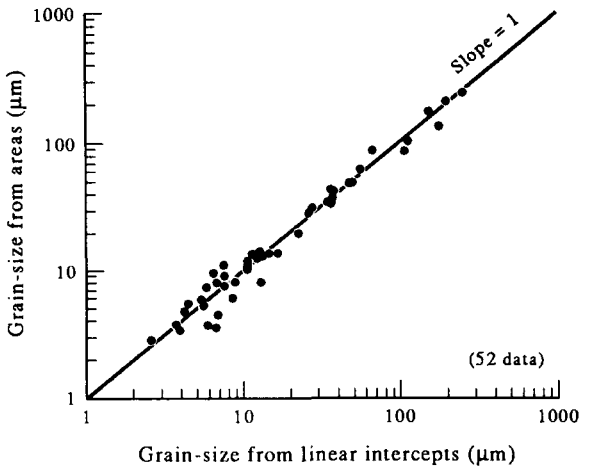

Fig. 4. The observed proportionality between mean planar grain diameter by the linear intercept method and the mean diameter of a circle with the same area as the mean grain area. No stereological modifications have been applied to the observed grain diameters.

(*e*), 024 and 116 were measured. The pole figure scans were combined to give an inverse pole figure using the harmonic method as described in Casey (1981). Expansion to order 12 was used.

For naturally deformed samples complete pole figures were measured using the combined reflection and transmission mode techniques. The symmetry of the pole figures was triclinic. The calculation of the orientation distribution was based on the same diffraction peaks as above and was carried out again using the harmonic method, with expansion to order 12.

For microstructural studies a second, ultrathin (about 3 μm) section was prepared, polished on each side. From optical photomicrographs, line drawings of the grain boundaries were made, each drawing typically containing 600–1200 grains. The drawings were digitized as bitmapped images using a scanner. From these images, grain boundaries were automatically digitized to form an array of co-ordinates for each grain. Using a procedure based on that described by Tough & Miles (1984) and Tough (1988), for each grain its centroid and area were found, together with a descriptor of its shape and orientation in terms of an ellipse. The planar distribution of grain size was then obtained by finding the diameter of the circle with the same area as each grain. Mean grain size was also found using the linear intercept technique. This was obtained automatically from the scanned image using a family of about 30–40 straight lines of different orientations transecting the image. The linear proportionality observed between grain diameters obtained using both methods is shown in Fig. 4. No stereological corrections have been applied to the planar (two-dimensional) grain sizes reported.

Overall two-dimensional strain was estimated from the measured grain shapes using the enhanced-normalized Fry (1979) method (Erslev 1988, Erslev & Ge 1990), wherein a best-fit strain ellipse is obtained by a least-squares procedure.

EXPERIMENTAL RESULTS

Mechanical properties

The test conditions of all experiments reported are shown in Table 1 and in Fig. 5 with respect to the various deformation mechanism fields for calcite. All samples deformed by fully ductile flow. At 300 and 500°C the flow is strain-hardening, giving way at higher temperatures to apparently steady flow over the 10–30% strain range for which stress–strain curves are meaningful. For the grain sizes used, the range of test conditions chosen spans the transition between grain-size insensitive, crystal-plastic deformation of calcite rocks at low temperatures and large grain sizes, through the regimes of grain-size sensitive flow at higher temperatures (Walker *et al.* 1990). The characteristics of strain-rate ($\dot{e}$) sensitivity to flow stress (σ) and grain size (d) in these various flow regimes are described by parameters n and m in the constitutive flow law, which may be written in the form

$$\dot{e} = A\sigma^n d^m,$$

in which A includes the effects of temperature and structure terms. For the synthetic aggregates used in this study, at high stresses (low temperatures, <600°C at laboratory strain-rates) $n = 5$–7 and $d = 0$ (i.e. grain-size insensitive flow). At intermediate stresses (higher temperatures, 600–700°C) the flow becomes grain-size sensitive, with $n = 3.3$ and $d = -1.3$, and at low stresses (700°C and above), $n = 1.7$ and $d = -1.9$. In fact, in calcite rocks the high-stress regime of nominally grain-size insensitive flow shows a grain-size sensitivity but of positive sign. This is due partially to the Hall–Petch effect but mainly to the fact that deformation by twinning becomes facilitated with increasing grain size (Rowe & Rutter 1990).

Grain growth

Above 650°C, for the typical time duration of these experiments, grain growth begins to be important in pure calcite rocks. Figure 6(a) shows log grain size as a function of log time at 700°C. This figure incorporates both the previously reported grain-size data of Walker *et al.* (1990) and the new data. No significant difference can be observed between samples coarsened under static conditions and those that coarsened during deformation provided the deformation remains in the grain-size sensitive field. In Fig. 6(b) planar grain-size distributions are collected together for the products of the 700°C runs, with square-root grain size (normalized by the mean grain size) plotted on the abscissa, and with the frequency normalized to a peak value of unity. The weighted average of each normalized grain-size class is also plotted, together with the best-fit Gaussian curve. Range bars for the standard deviation of the best-fit Gaussians to each of the data sets from individual specimens show how closely the individual best-fit curves coincide with each other. It has previously been argued that for normal grain growth of many metals

Table 1. Summary of experiments performed for which X-ray texture analyses were carried out. Synthetic samples are prefixed L, Carrara marble samples are prefixed CR and Solnhofen limestone samples are prefixed SOL. Compression tests are indicated by positive figures for strain and strain-rate, and vice versa for extension tests. Strains are reported as conventional engineering strain, and the engineering strain rate and differential stress is that prevailing at 10% strain. In the cold-press column, 'iso' means truly isostatic cold-pressing at 200 MPa, 'uni' signifies uniaxial cold-pressing at 600 MPa end-pressure in a die. Total time is time at maximum temperature. For the deformed synthetic samples the maximum temperature was always 700°C. Grain sizes are reported as the mean with ±1 SD. Grain shapes (grain-shape factor) were measured by the enhanced normalized Fry method, and where uncertainties are quoted these are ranges arising from variations of the selected scale length and selection factor. For comparison, grain shapes expected assuming homogeneous plastic strain (sample shape factor) are also given. Strain estimated in the centre of each sample from grain shape is usually higher than bulk strain shape factor owing to low strains adjacent to the loading pistons. Initial grain size estimated for undeformed Carrara marble is probably anomalously low owing to a very large sample size (1300 grains), giving additional weight to the smaller sized grains

Spec no.	Cold-press	Temperature (°C)	Initial grain size (μm)	Final grain size (μm)	Confining pressure (MPa)	Total strain (%)	Time at maximum temperature (h)	Strain rate (s^{-1})	Stress (MPa)	Shape factor	
										Grain	Sample
Heat-treated only, no deformation											
L1	uni	530	3.4 ± 0.6	3.0 ± 0.5	300	0	3.5	—	—	1.06 ± 0.01	—
L2	iso	530	3.4 ± 0.6	2.1 ± 0.5	300	0	3.5	—	—	1.19 ± 0.02	—
L13	uni	700	3.4 ± 0.6	9.0 ± 1.8	300	0	3.0	—	—	1.06	—
L14	iso	700	3.4 ± 0.6	9.4 ± 0.9	200	0	3.0	—	—	1.17	—
L16	iso	700	3.4 ± 0.6	7.8 ± 1.2	200	0	1.0	—	—	1.05	—
L17	iso	630	3.4 ± 0.6	3.5 ± 0.8	200	0	1.0	—	—	1.14	—
Plastic deformation at high stresses–low temperatures											
L4	iso	500	7.5 ± 0.8	8.3 ± 2.4	200	+30	15	-3×10^{-4}	205	1.91 ± 0.02	1.62
L12	iso	600	7.5 ± 0.8	11 ± 1.3	200	+18	4.0	$+3 \times 10^{-4}$	120	1.22	1.32
CR41	—	500	130 ± 25	174 ± 57	350	−24	2.0	-8.3×10^{-5}	260	1.83	1.42
CR19a	—	600	130 ± 25	182 ± 42	280	−25	2.0	-3×10^{-4}	150	1.73	1.45
L37	iso	600	38 ± 6	57 ± 14	350	−34	14.2	-6×10^{-5}	90	1.44	1.65
Grain-size sensitive flow regime											
L27	iso	700	7.5 ± 0.8	14.1 ± 2.5	200	+28	23	$+3 \times 10^{-6}$	20	1.21	1.57
L28	uni	700	3.4 ± 0.3	13.4 ± 1.9	250	−31.5	33	-3×10^{-6}	28	1.24	1.59
L29	iso	700	7.5 ± 0.8	—	250	−25.4	28.8	-3×10^{-6}	26		1.45
L30	iso	700	7.5 ± 0.8	12.8 ± 1.8	250	−30.5	34.5	-3×10^{-6}	12	1.06	1.57
L11	iso	700	7.5 ± 0.8	15.3 ± 7.9	200	−27	6.2	$+3 \times 10^{-5}$	30	1.19 ± 0.04	1.54
L23	iso	700	3.4 ± 0.3	6.0 ± 1.1	270	−33	1.8	-6×10^{-5}	55	1.30	1.62
L24a (end)	iso	700	3.4 ± 0.3	7.1 ± 1.1	270	−50	3.5	-7×10^{-5}	~50	1.08	2.12
L24b (neck)	iso	700	3.4 ± 0.3	7.3 ± 1.5	270	−600	3.5	-5×10^{-4}	~70	1.63	14.7
SOL1	—	800	3.8 ± 0.3	5.3 ± 1.0	200	+33	2.5	$+8 \times 10^{-5}$	15	1.16	1.62
SOL2	—	700	3.8 ± 0.3	3.8 ± 1.9	200	+30.5	1.1	$+8 \times 10^{-5}$	62	1.37	1.64
SOL3	—	900	3.8 ± 0.3	10.4 ± 1.8	200	+32.9	1.1	$+8 \times 10^{-5}$	5.1	1.02	1.72
SOL4	—	700	3.8 ± 0.3	5.4 ± 1.1	300	−47	2.0	-8×10^{-5}	106	1.21	2.02
Compound deformation and heat-treatment histories											
L34	iso	700+	7.5 ± 0.8		200		1.0		—		
		300		13.5 ± 3.0		+12		$+8 \times 10^{-5}$	450	1.32	1.20
L35	iso	700+	7.5 ± 0.8		200		1.5		—		
		300+				+12		$+8 \times 10^{-5}$	450		1.20
		700		23.6 ± 5.1			1.7		—	1.11	1.20
L36	iso	700+	7.5 ± 0.8		200		1.0		—		
		300+				+12		$+8 \times 10^{-5}$	450		1.20
		700+					1.0				
		700		24.0 ± 5.1		+25.5	4.0	$+1.4 \times 10^{-5}$	58	1.27	1.50
SOL5	–	300+	3.8 ± 0.3		200	+12.5		$+8 \times 10^{-5}$	490		1.20
		700+					0.8				
		700		4.7 ± 1.0		+42.8	4.4	$+2 \times 10^{-5}$	22	1.12	2.10

(e.g. Andrade & Aboav 1966, Aboav & Langdon 1973) that such a plot is strictly Gaussian, and our new data now demonstrate that this is also a good description of the planar distribution of grain size for both static and dynamic grain growth in pure, dry calcite rocks. From computer simulations of normal grain growth, Anderson & Grest (1989) show that a generalized Louat function should provide a slightly better description of the planar distribution of grain size than a Gaussian fit to square root grain size. Whilst the normalized grain-size distribution remains of constant form during grain growth, Fig. 6(a) shows how the mean grain size, and hence the distribution curve itself, is displaced to larger grain sizes with time.

The tests on pure calcite aggregate at low strain-rates at 700°C, where the flow is grain-size sensitive, showed hardening due to grain coarsening. Indeed, it is not practical to extend tests on pure, fine-grained calcite rocks to higher temperatures owing to the rapidity with which grain growth modifies the microstructure. Figure 6(a) shows how the small amounts of intergranular impurities that are found in Solnhofen limestone dramatically reduce grain growth kinetics. This has meant that we have been able to perform deformation tests at temperatures up to 900°C of Solnhofen limestone without serious problems from grain growth.

Deformation microstructures and preferred crystallographic orientation

These data have been grouped as follows:

(a) crystallographic fabrics and microstructures produced by grain-size insensitive crystal-plastic flow;

(b) comparative crystallographic fabrics of samples

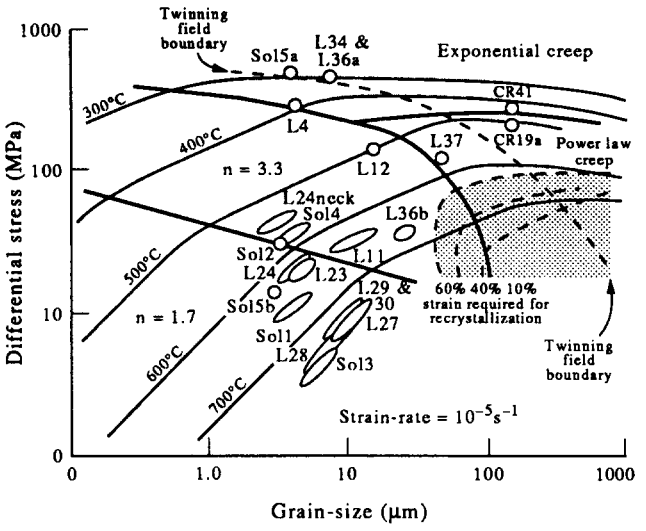

Fig. 5. Deformation mechanism map (based on data of Walker *et al.* 1990) for pure calcite rocks showing the relative positions of each of the specimens for which crystallographic fabrics have been measured. The elongate shape of the symbols representing principally the finer-grained samples at the higher temperatures indicates the grain growth that occurred during the course of the test. The initial grain size lies at the lower left of an elongate symbol, the final grain size at the upper right. Isotherms are plotted for a strain rate of 10^{-5} s^{-1}. Samples deformed at other strain-rates have been plotted on this plane by using temperature to compensate for strain-rate differences. The position of the mechanism field boundaries (shown as emboldened lines) is little affected by strain-rate variations over the experimental range. The shaded area shows the range of conditions leading to microstructure modification (usually grain-size reduction) by dynamic recrystallization (unpublished data of Rutter 1993).

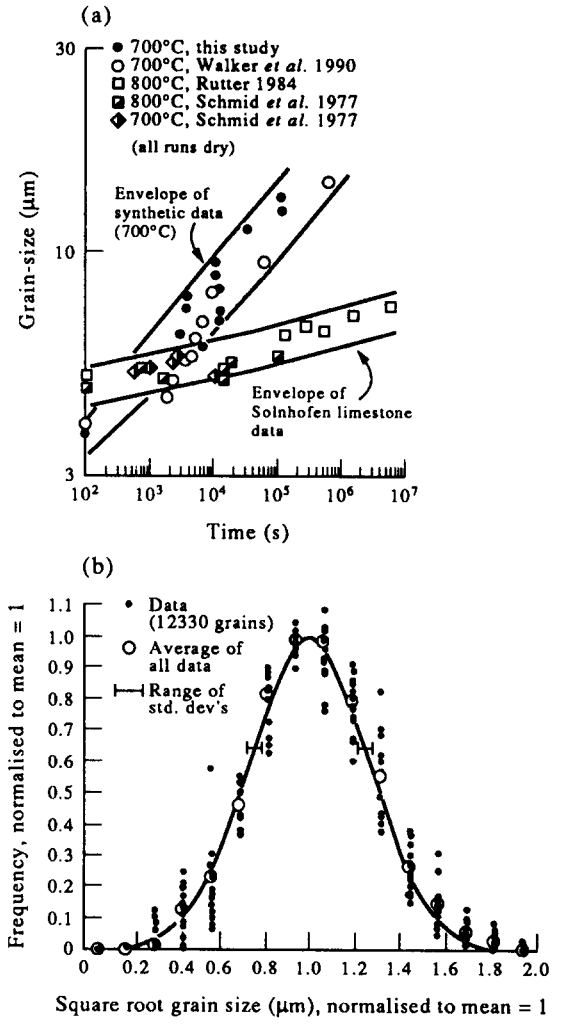

Fig. 6. Grain growth behaviour of calcite rocks. (a) Plot of log planar mean grain size vs log time-at-temperature for both static and dynamic grain growth of pure, dry, synthetic calcite rocks at 700°C (this study and data of Walker *et al.* 1990). Data for dry Solnhofen limestone at 700 and 800°C (Schmid *et al.* 1977, Rutter 1984) demonstrate the inhibition of grain growth by intergranular second phases. Mean grain diameter was calculated from measured areas. Envelopes of data points indicate the range of values about the mean grain size. (b) Normalized planar distribution of square-root grain size for all runs at 700°C on pure, synthetic hot-pressed calcite samples. Data are normalized to unit mean grain size by division by the mean value for each specimen, and to a peak frequency of unity for the best-fit Gaussian distribution for each specimen. Open circles show the average values of class divisions weighted according to number of grains contributing to the class, and small filled circles show data from individual specimens. The Gaussian curve shown is the best-fit to the open circles. Range bars for the standard deviations of best fit curves to distributions for the individual specimens show how similar are all of the curves to each other.

made by uniaxial and isotropic loading respectively in the cold-pressing stage, but not subsequently hot-deformed;

(c) crystallographic fabrics and microstructures produced during high-stress, grain-size sensitive flow (600°C and at 700°C at high strain-rates), including the effects of extensional strains up to *ca* 1000%;

(d) crystallographic fabrics and microstructures produced during low-stress, grain-size sensitive flow (slow deformation at 700°C and at higher temperatures) in synthetic, hot-pressed samples and in Solnhofen limestone; and

(e) crystallographic fabrics and microstructure produced during annealing recrystallization following cold-work at 300°C, and after a further episode of crystal-plastic or grain-size sensitive flow at high temperature.

Fabric data for the experimentally deformed samples are most conveniently presented as inverse pole figures for the unique specimen axis (compression or extension direction, respectively) on a 60° sector of the upper-hemisphere equal-area projection for calcite. The labelling convention of the common crystallographic forms is shown in Fig. 7.

(a) Crystallographic fabrics of grain-size insensitive intracrystalline plastic flow. Fabric types are most conveniently described by comparison with the common types produced during the respectively low- and high-temperature intracrystalline flow of calcite rocks (Casey *et al.* 1978, Spiers 1979). These are illustrated in Fig. 7, for the cases of uniaxial extension and compression. The low-temperature (high stress, twinning active) fabric in compression (specimen L34) is characterized by a strong maximum of poles to *e*, the twin plane, and is termed the *e* fabric. There is generally a weaker shoulder towards *c*. The intensity of this fabric can become very marked, and is half as strong (more than 7 times uniform around *e*) as it will ever become after only about 12% strain (Owens & Rutter 1978). There is commonly a marked minimum around *f*, where the maximum resolved shear stress would occur on the *e* plane in its slip direction. The corresponding extensional fabric is illustrated by speci-

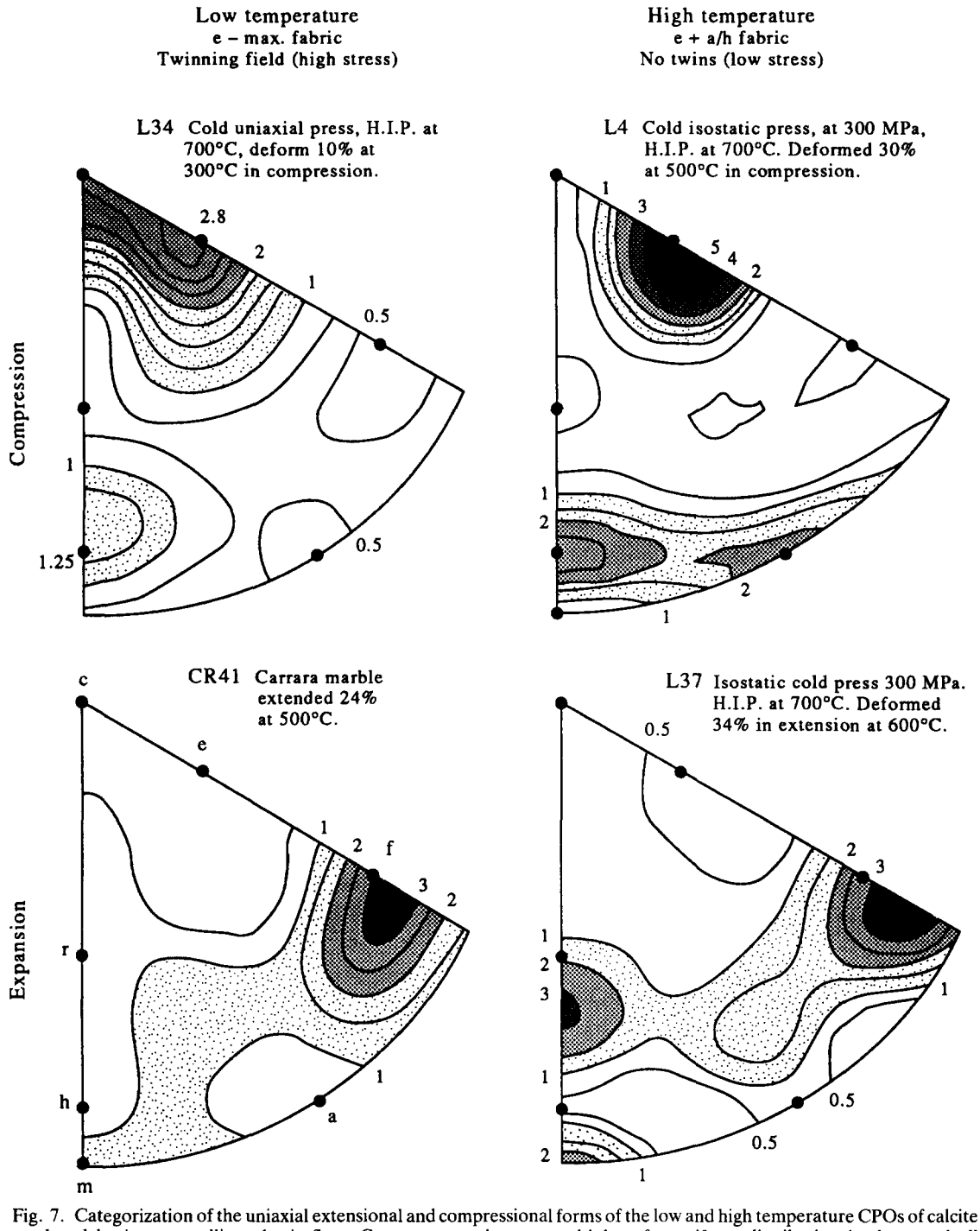

Fig. 7. Categorization of the uniaxial extensional and compressional forms of the low and high temperature CPOs of calcite produced by intracrystalline plastic flow. Contours are given as multiples of a uniform distribution in these and all subsequent inverse pole figures. The commonly adopted labelling scheme for crystallographic forms and crystallographic axes of calcite are shown on the figure for CR41. Experimental details are given in Table 1.

men CR41. The coarser marble was used here because twinning remains active to higher temperatures and hence lower flow stresses. The fabric is marked by a single maximum close to *f*. The *e* fabric is the expected fabric type in compression if deformation is dominated by slip on two *r* planes plus *e* twinning (Wenk *et al.* 1973). Spiers (1979) showed that formation of this fabric is accompanied by marked strain heterogeneity on the grain scale.

The single maxima in these low-temperature (high-stress) fabrics mean that there is a single end orientation to which grains tend, and these are shown in Fig. 8 for the extensional and compressional cases as the complete orientation of a single grain relative to the unique deformation axis. In extension, a single *f* maximum in the extension direction leaves the two active *e* planes forming a girdle almost normal to the extension direction, whereas in compression the maximum of the single most active *e* plane parallel to the compression direction leaves two *f* planes normal to compression.

The high-temperature (lower stress, twinning inactive) fabric is more complex, with more than a single maximum on the inverse pole figure. Therefore it cannot be represented simply by the orientation of a single

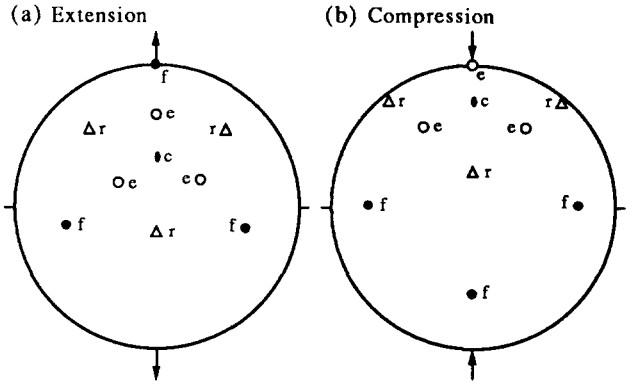

Fig. 8. The end-point orientations of the twinning-active, low-temperature, high-stress fabric type in extension (*f*-maximum fabric) and compression (*e*-maximum fabric), illustrated using the orientation of a single crystallite with respect to the unique deformation axis. The complete family of axisymmetric pole figures would be generated by spinning the crystallite about the unique axis and inverting it about the same axis.

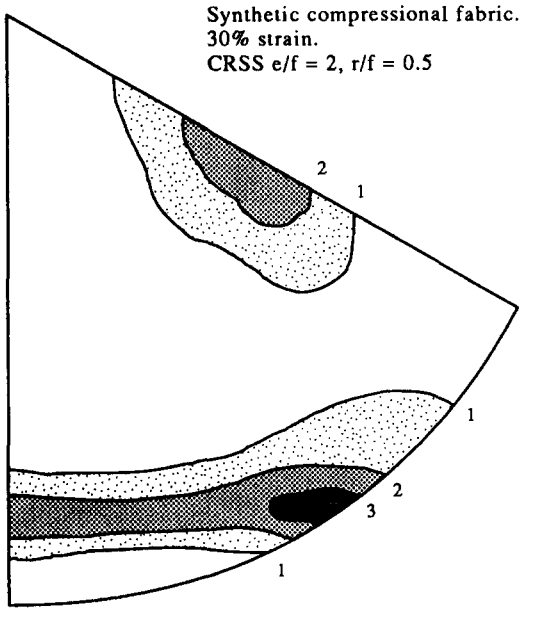

Fig. 9. Inverse pole figure for an *e* + *a/h* fabric synthesized using the Taylor–Bishop–Hill analysis with critical resolved shear stress (CRSS) ratios *e/f* = 2.0 and *r/f* = 0.5 (after Lister 1978). The inverse rotation diagram has been integrated over a 30% uniaxial shortening strain. *e* twinning was treated as a slip system in this analysis. This was the only combination of CRSS values which came close to predicting the observed homogeneous strain fabric type.

crystal on the pole figure. In compression it shows a weaker maximum close to *e* with a distinct girdle between *h* and *a*, hence is termed the *e* + *a/h* fabric. Typical examples obtained in the present study of the uniaxial compression and extension forms of these are shown in Fig. 7 (L4 and L37). The extensional fabric appears to be approximately the inverse of the compressional one.

The transition between the *e* and *e* + *a/h* fabrics is marked by the temperature above which twinning is disabled and the deformation switches from approximately homogeneous stress at the grain-scale to homogeneous strain (Spiers 1979). Lister (1978) successfully modelled the development of this fabric using the fully-constrained Taylor–Bishop–Hill analysis, which presumes homogeneous strain at the grain-scale. The fabric integrated over a 30% finite uniaxial shortening that closely matches the experimental fabric is shown in Fig. 9.

Because the resistance to twinning is grain-size sensitive (Rowe & Rutter 1990), so too is the transition temperature between the two crystal-plastic fabric types. For example, it occurs at about 350°C at a grain size of about 5 μm, rising to about 650°C at a grain size of 150 μm. The low-temperature (twinning active) type of fabric is that which is commonly found in calcite tectonites. We are unaware of any recorded occurrence in nature of a CPO which corresponds to the high-temperature (twinning absent) type.

The characteristic microstructures of samples deformed crystal-plastically in compression in each of these two flow regimes may be compared in Fig. 2(c) (specimen L4, twinning inactive) and Fig. 3(a) (specimen L34, twinning active).

(b) Fabric of the synthetic, fine-grained starting materials. Figure 10 shows that sample fabrication by truly isotropic cold and hot pressing produces an effectively uniform CPO. As might be expected, however, uniaxial cold pressing (with the lateral constraint of the die) prior to hot pressing results in a CPO, in this case a weak *c*-maximum.

(c) Fabrics produced during high-stress, grain-size sensitive flow (the n = 3.3, m = −1.3 *regime).* Behaviour in this regime is illustrated by reference to sample L24, deformed in extension at 700°C (Fig. 11). Although the bulk extensional strain was only 105%, the non-linearity of the flow was sufficient to provoke the formation of a neck, in the centre of which the strain attained a maximum of about 1100% extension. CPOs were obtained from near to the neck, where the strain was on average 600% or larger, and in the vicinity of the loading piston where the extensional strain was about 50%. Figure 11 shows the IPFs obtained, together with the grain shapes relative to the local bulk strain ellipses. Figures 2(d) & (e) show optical micrographs at 50% and about 1000% extension, respectively.

For each section the grain-shape fabric remains weak, attaining a stable shape factor of only about 1.5:1 after 1000% extension. The mean planar grain size was unaffected by the large strain variation. In our previous study (Walker *et al.* 1990) we have shown from the microscopy of polished split specimens that grain boundary sliding is an important deformation mechanism during flow under these conditions. This, together with constancy of grain size over a large strain range, suggests that there is no significant modification of the grain microstructure by grain boundary migration during the flow.

It should be noted that care must be taken in the interpretation of planar grain sizes in specimens deformed to large, non-plane strains such as these. If the grain shape tracks the bulk strain, apparent grain size

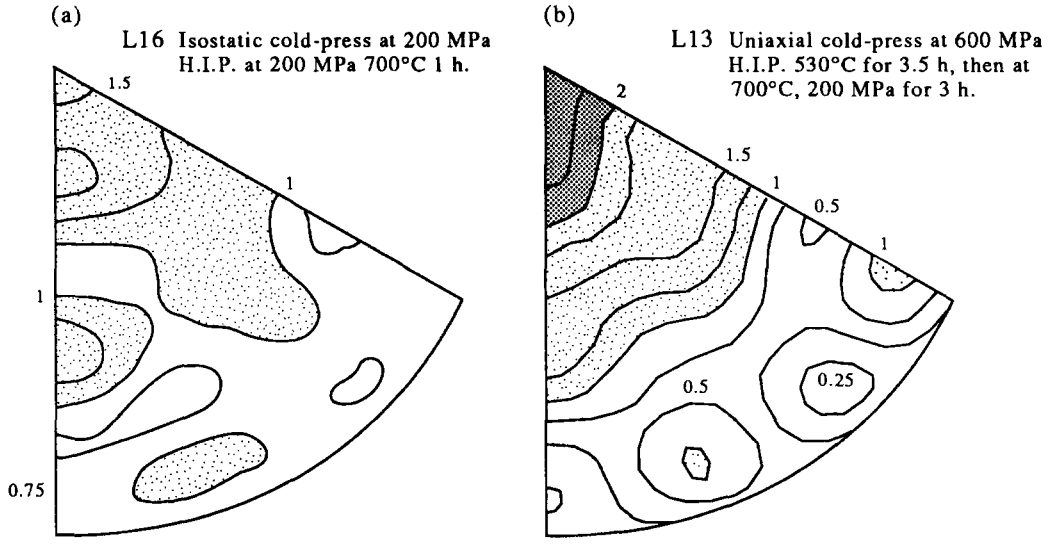

Fig. 10. Comparative inverse pole figures of synthetic samples prior to high-temperature deformation (starting materials). (a) A specimen fabricated by isostatic cold and hot pressing. The CPO is effectively uniform. (b) A specimen fabricated by initially uniaxial cold pressing in a die, followed by hot isostatic pressing. A weak *c*-maximum crystallographic fabric has resulted.

increases during extension and decreases during compression, owing to the movement of material respectively into or out of the plane of the section. It is a simple matter to compute the expected change. In this case, however, the maintenance of a weak grain-shape factor means that planar distributions of grain size can be compared, even between samples having suffered widely disparate bulk strains.

The sequence of IPFs (Fig. 11) shows that after 50% extension (normally a large strain by experimental standards) only a weak CPO has developed. There is a weak maximum towards the periphery of the projection, corresponding to a *c*- or *e*-maximum in the compression direction. The intensity is, however, not far above the noise level. This would normally lead to the conclusion that superplastic flow does not lead to significant CPO development. After more than 600% extension, however, a substantial CPO has developed. It is of essentially the same type as in the twinning-absent intracrystalline flow regime. Its existence is easily discernible on a flat-stage optical microscope and the fabric corresponds to the *e* + *a*/*h* type. It must be concluded, therefore, that although the fabric develops much more slowly than in the regime of grain-size insensitive intracrystalline plasticity, it will be significant when the large strains typical of natural shear zones are taken into account.

(d) Crystallographic fabrics produced during low-stress, grain-size sensitive flow (the n = 1.7, m = −1.9 *flow regime).* In these pure, synthetic calcite rocks, grain growth is highly competitive with flow in this regime, so that high strains cannot be attained without excessive growth. The grain growth causes concomitant strain-hardening, owing to the grain-size sensitive nature of the flow. The hardening, coupled with the low *n* value also eliminates the tendency towards necking in extension, thus deformed specimens were always parallel-sided and local strains did not exceed the bulk strain. Compressional and extensional fabrics produced in this regime are shown in Fig. 12. The fabrics are weak even after *ca* 30% strain, but are discernibly similar to the high-temperature crystal-plastic types. Initial and final grain sizes listed in Table 1 show the extent of grain growth in individual runs.

Owing to the problems of grain growth in pure calcite rocks restricting access to high strains in this flow regime, for comparison we have additionally deformed four samples of Solnhofen limestone [from the same block as used by Rutter (1972, 1974)], in extension at 700°C and in compression at 700, 800 and 900°C. The few percent of second phase impurities in the grain boundaries exert a powerful inhibiting effect on grain-growth kinetics (Fig. 6), even up to 900°C. Grain growth did not, however, eliminate the tendency for extended specimens to remain parallel sided in extension. Furthermore, tests in compression in the gas-medium machine could not go to very high strains because the long, laterally unsupported axial column tends to buckling instabilities. Nevertheless, the compression tests on Solnhofen limestone have been carried out to a little over 30% shortening, similar to what was attained in extension.

The results obtained from Solnhofen limestone samples are shown in Fig. 13. In all samples, whether of hot-pressed pure calcite or of Solnhofen limestone, up to 30% strain the fabric is weak, with intensities little above background. In this respect they are entirely comparable with necked sample L24 (Fig. 11), which showed a very slow rate of fabric development, but which was significant over a very large strain. The fabrics all tend to show a weak intensification towards the periphery of the projection. For Solnhofen limestone this applies both for extension and compression. The extended pure samples behaved similarly, but compressed pure sample L27 shows a weak tendency to a girdle from *r* to a position between *e* and *f* (Fig. 12). On the basis of the

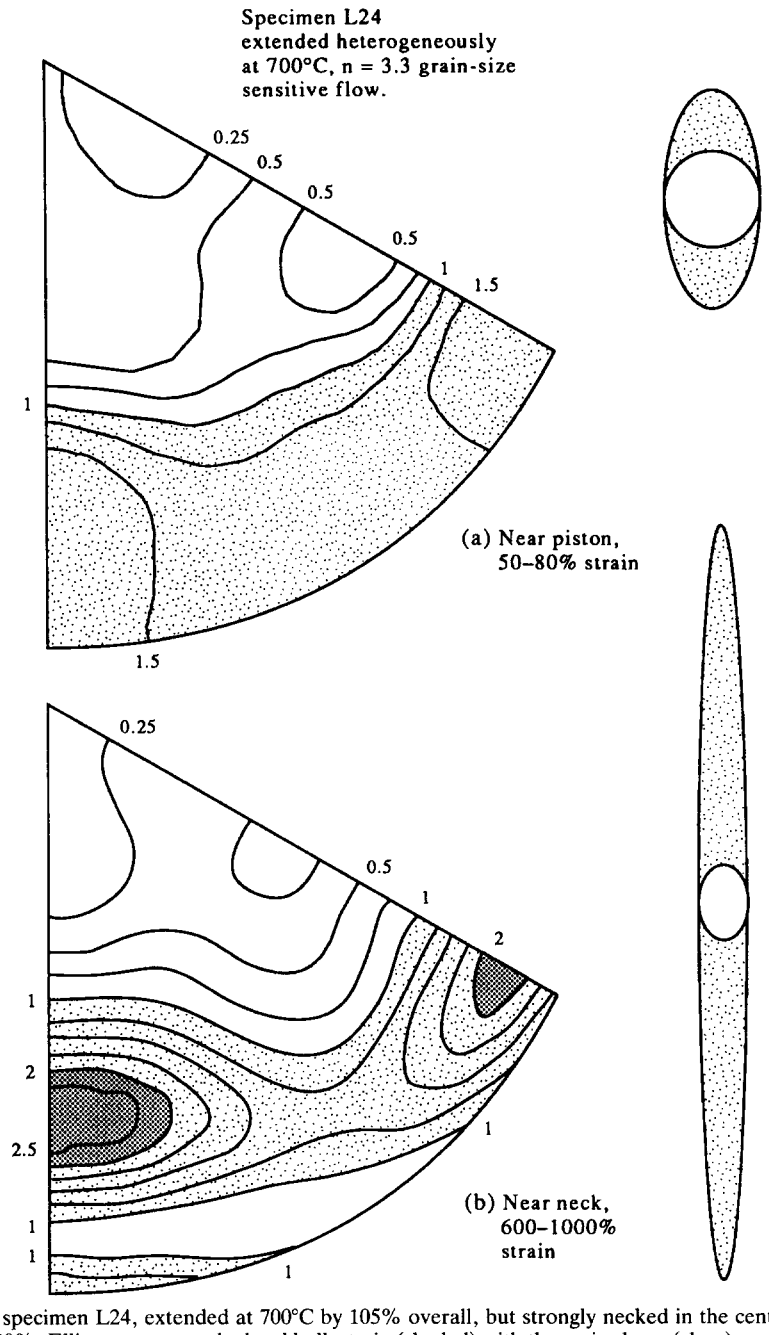

Fig. 11. Data for specimen L24, extended at 700°C by 105% overall, but strongly necked in the centre, where the local strain attained 1100%. Ellipses compare the local bulk strain (shaded) with the grain shape (clear) near the loading piston and near the neck, respectively. Inverse pole figures are shown for these positions in the sample. The CPO develops much more slowly than in the high-temperature intracrystalline plastic field, but is of the same (e + a/h) type.

available data it is impossible to conclude whether or not significant CPO will develop during the flow of calcite rocks to large strains in this flow regime, but it would clearly be unwise to use presence of a CPO alone in a natural high-strain zone to infer that the flow was dominated by intracrystalline plasticity rather than by grain boundary sliding.

Microstructures produced by flow in this regime are equigranular foam structures, free of intragranular strain features, exactly as seen in samples deformed in the higher stress grain-size sensitive regime at comparable strains (Fig. 2f).

(e) Fabrics produced during initial crystal-plastic deformation at high stress, followed by annealing recrystallization and subsequent hot working. The aims here are: (a) to investigate the extent to which an initial low-temperature, high-stress CPO survives an annealing recrystallization which removes microstructural evidence of the earlier deformation history; and (b) to investigate how subsequent coaxial hot-working modifies the CPO. Using a synthetic, hot pressed sample, an e-maximum fabric was impressed by 12% deformation at 300°C in compression (specimen L34, CPO shown in Fig. 14, microstructure in Fig. 3a). The microstructure is characterized by grain flattening and twinning.

The same treatment was applied to specimen L35, followed by 2 h annealing at 700°C. The CPO is also shown in Fig. 14. The annealing recrystallization restored the microstructure to the equigranular foam

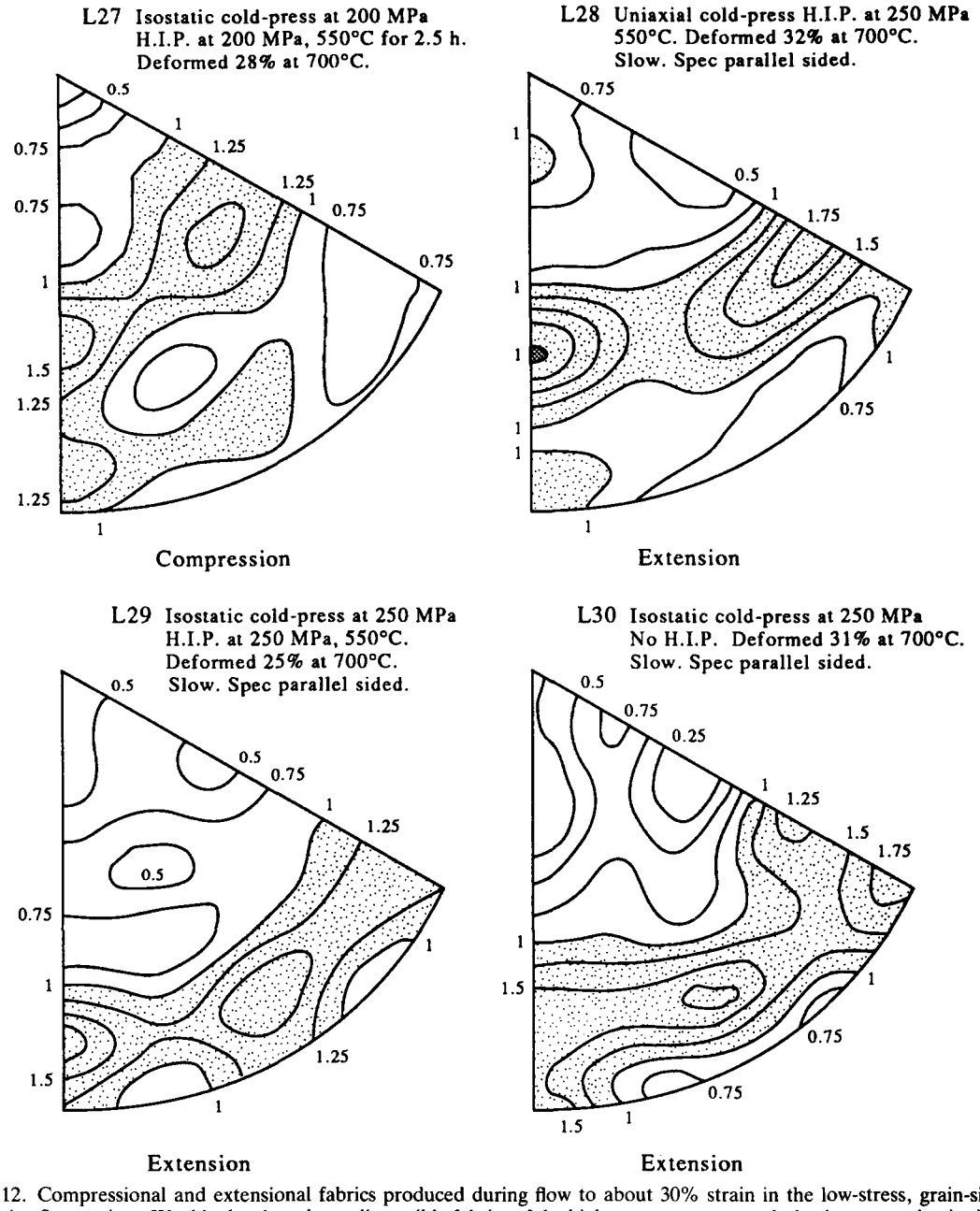

Fig. 12. Compressional and extensional fabrics produced during flow to about 30% strain in the low-stress, grain-size sensitive flow regime. Weakly developed, yet discernible fabrics of the high temperature crystal-plastic type are beginning to develop.

structure. This recrystallization proceeds mainly by twin boundary migration, accompanied and followed by a certain amount of grain growth. Total recrystallization by twin boundary migration has been followed in detail in the experimental deformation of Carrara marble (Rutter unpublished work). It is clearly a powerful process of microstructural readjustment in calcite rocks (see also Schmid *et al.* 1987). For an *e*-maximum CPO, replacement of host grain volume by twinned volume does not modify an axisymmetric fabric. Hence, as anticipated, the recrystallization does not significantly modify or weaken the CPO. Thus calcite rocks initially deformed in the twinning regime and subsequently recrystallized by twin boundary migration, would be expected to show no *microstructural* evidence of twinning, yet preserve evidence of the earlier history in the inherited CPO. As pointed out in the introduction, this is commonly observed.

In specimen L36 (Fig. 14), static annealing at 700°C was followed by a second stage of deformation, by 20% in compression at 700°C. The combined effect of annealing after cold-working and time-at-temperature during hot working caused the initial grain size of *ca* 13 μm to increase to 24 μm. Thus the second deformation occurred largely in the regime of high-stress, grain-size sensitive flow. In the CPO, the *e*-maximum has moved slightly outwards to the position expected for the *e* + *a*/*h* fabric, but the *a*/*h* girdle has not been able fully to develop. This suggests that once density has been accumulated in the inner part of the projection, it cannot be transferred across the *r*/*f* divide; hence during the second deformation there are too few crystallites avail-

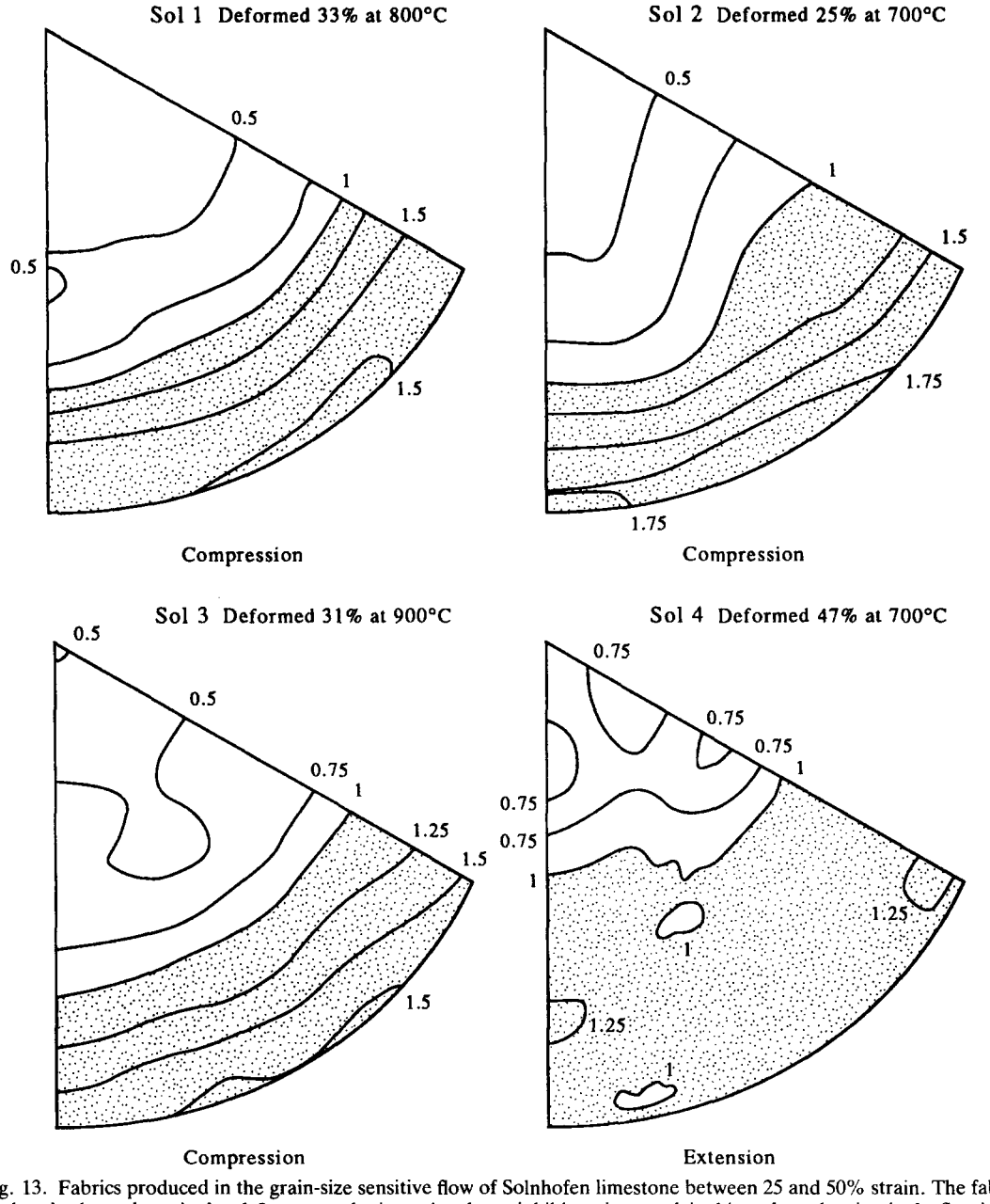

Fig. 13. Fabrics produced in the grain-size sensitive flow of Solnhofen limestone between 25 and 50% strain. The fabrics are barely above the noise level. Intergranular impurity phases inhibit grain growth in this rock, and maintain the flow in the grain-size sensitive field, so that the rate of fabric development is very slow over the accessible strain range.

able in suitable orientations for the complete *a/h* girdle to form.

In order to investigate the effect of the second deformation being in the low-stress, grain-size sensitive regime, a Solnhofen limestone specimen (So15) was given the same two-stage deformation treatment as L36, with 30% shortening in the second stage. Once again, the CPO (Fig. 14) shows how the early fabric survives reworking in the superplastic field, this time with little grain growth.

CONCLUSIONS AND GEOLOGICAL IMPLICATIONS OF RESULTS

For the flow of calcite rocks by intracrystalline plasticity, we have confirmed the transition from the *e*-maximum to the *e* + *a/h* type with decreasing flow stress (increasing temperature). This occurs at the flow stress below which mechanical twinning ceases to be important. We have characterized these fabric types both in uniaxial compression and in extension.

We have shown that in the grain-size sensitive flow of fine-grained calcite rocks, under conditions whereby an equigranular or nearly equigranular microstructure persists to high strains, CPO still develops, but at a much lower rate than in the regime of intracrystalline plasticity. The rate of CPO development is lower as the flow stress is lowered. Schmid *et al.* (1987) arrived at the same conclusions from simple shear experiments on calcite rocks during grain-size sensitive flow. A fabric which is still insignificant after 50% strain may become substantial after 1000% strain, however. Under these conditions, it is known from previous studies that the flow is

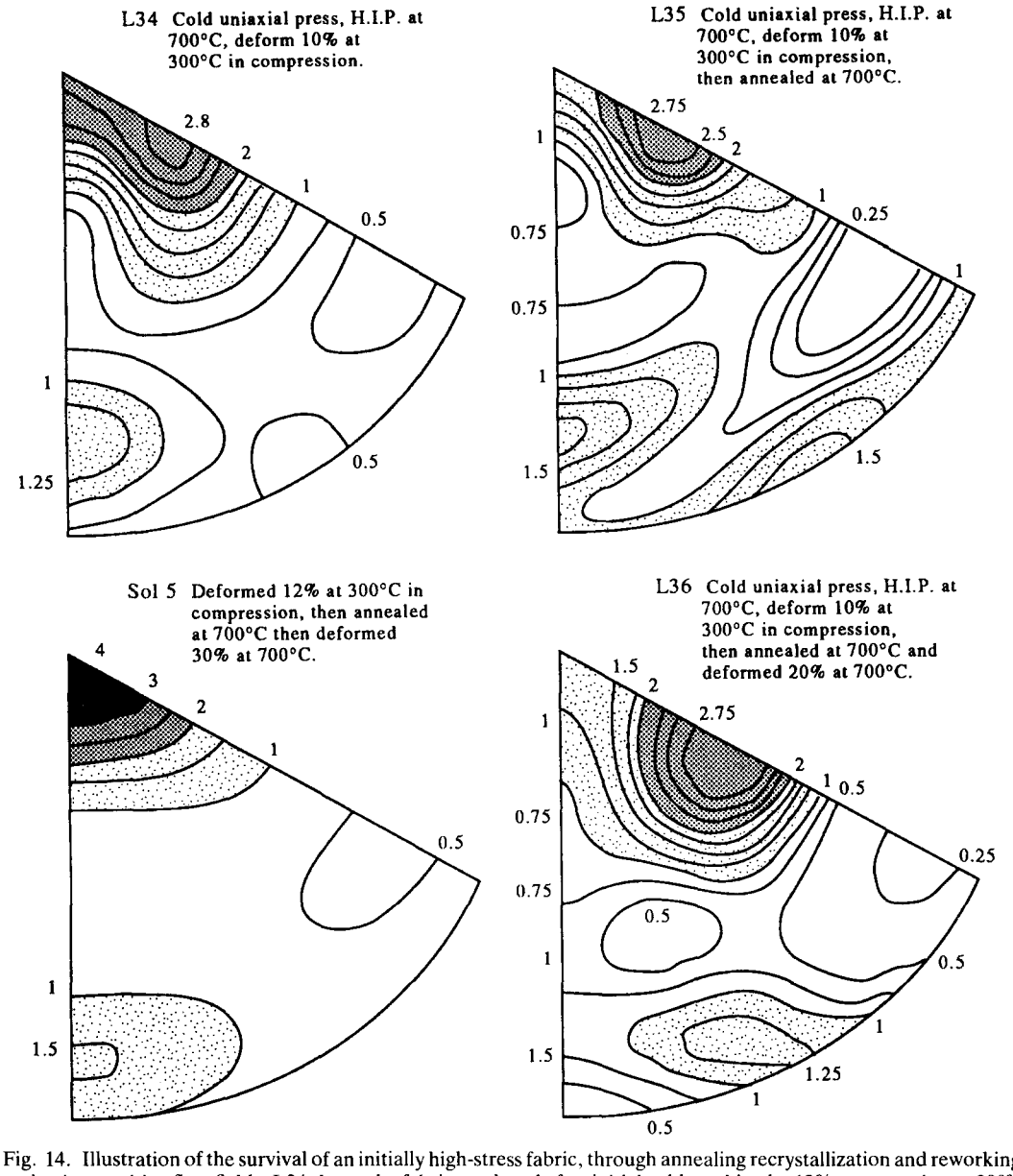

Fig. 14. Illustration of the survival of an initially high-stress fabric, through annealing recrystallization and reworking in the grain-size sensitive flow fields. L34 shows the fabric produced after initial cold-working by 12% compression at 300°C. L35 shows how the fabric is little modified after a further 700°C annealing recrystallization for 2 h, despite grain growth which increased the grain size several-fold. In L36 a further 20% compression in the high-stress grain-size sensitive flow field was applied after annealing. The initial *e*-maximum moves slightly further away from *c*, and there is an attempt to generate the *a*/*h* girdle from what little intensity exists near the periphery of the projection. In So15 the high-temperature reworking was in the low-stress grain-size sensitive (superplastic) flow field, because relatively little grain growth occurs in Solnhofen limestone. Thirty percent hot-working in compression has not significantly modified the original low-temperature fabric (compared with L34).

dominated by grain-boundary sliding accommodated by a mixture of diffusion and crystal-plasticity (superplastic flow). Thus the presence of a CPO in intensely deformed, fine-grained calcite rocks cannot be considered diagnostic only of intracrystalline plastic flow, or of flow involving continuous or cyclic dynamic recrystallization, to the exclusion of grain-boundary sliding. This conclusion may also be broadly applicable to other rock types.

Apart from the possibility of the production of a 'primary' CPO during superplastic flow, we have also shown that an early-formed fabric may persist through an episode of recrystallization. Thus during the crystal-plastic deformation under high stress of a shear zone protolith, a low-temperature type of fabric involving twinning might develop. The twinned microstructure would be expected to be removed by twin boundary migration as an initial stage of dynamic recrystallization, perhaps even before any grain-size reduction occurs. This will preserve an *e*-maximum type of fabric, or its equivalent for a different strain path. Although we have not yet demonstrated it directly, it is anticipated that through subgrain rotation-recrystallization and grain-size reduction the primary CPO will be substantially preserved. Some type of modified initial fabric is likely to survive any grain-boundary migration recrystallization, as demonstrated by Schmid *et al.* (1987). From the experiments on Solnhofen limestone it is clear that the

early fabric will tend to survive continued flow by grain-boundary sliding. This, we suggest, explains the common occurrence of low-temperature (*e*-maximum) fabrics in calcite ultramylonites.

Acknowledgements—This work was carried out with grant aid from the U.K. Natural Environment Research Council (GR3/6174). Visits to Manchester by L. Burlini were supported by the British Council and the Italian CNR. Experimental officer Robert Holloway helped keep the experimental equipment in running order and modified the two testing machines so that extension tests could be carried out. The work has benefited from discussions with S. J. Covey-Crump and R. Ward, S. J. Covey-Crump and P. Evans helped develop the computer program GRAINS for image processing. Professor Stefan Schmid provided a constructive review.

REFERENCES

Aboav, D. A. & Langdon, T. G. 1973. The planar distribution of grain-size in a polycrystalline ceramic. *Metallography* **6**, 9–15.

Andrade, E. N. da C. & Aboav, D. A. 1966. Grain-growth of metals of close-packed hexagonal structure. *Proc. R. Soc. Lond.* **A291**, 18–40.

Anderson, M. P. & Grest, G. S. 1989. Computer simulation of normal grain growth in three dimensions. *Phil. Mag.* **59B**, 293–329.

Behrmann, J. H. & Mainprice, D. H. 1987. Deformation mechanisms in a high temperature quartz–feldspar mylonite: evidence for superplastic flow in the lower continental crust. *Tectonophysics* **140**, 297–305.

Boullier, A. M. & Gueguen, Y. 1975. Origin of some mylonites by superplastic flow. *Contr. Miner. Petrol.* **50**, 93–104.

Bowen, A. W. & Hirsch, J. 1988. Texture changes in superplastically deformed aluminium alloys. In: *Proc. Eighth International Conference on Textures of Materials* (edited by Kallend, J. S. & Gottstein, G.). The Metallurgical Society, 549–554.

Casey, M. 1981. Numerical analysis of X-ray texture data: an implementation in FORTRAN allowing triclinic or axial specimen symmetry and most crystal symmetries. *Tectonophysics* **78**, 51–64.

Casey, M., Rutter, E. H., Schmid, S. M., Siddans, A. W. B. & Whalley, J. S. 1978. Texture development in experimentally deformed calcite rocks. In: *Proc. Conf. on Textures of Materials, Vol. II, Aachen* (edited by Gottstein, G. & Lücke, K.). 231–240.

Covey-Crump, S. J. & Rutter E. H. 1989. Thermally induced grain growth of calcite marbles on Naxos Island, Greece. *Contr. Miner. Petrol.* **101**, 69–86.

Erslev, E. A. 1988. Normalized center to center strain analysis of packed aggregates. *J. Struct. Geol.* **10**, 201–209.

Erslev, E. A. & Ge, H. 1990. Least squares center to center and mean object ellipse fabric analysis. *J. Struct. Geol.* **12**, 1047–1059.

Fry, N. 1979. Random point distributions and strain measurement in rocks. *Tectonophysics* **60**, 806–807.

Heard, H. C. 1963. Effect of large changes in strain rate in the experimental deformation of Yule marble. *J. Geol.* **71**, 162–195.

Heard, H. C. & Raleigh, C. B. 1972. Steady-state flow in marble at 500 to 800°C. *Bull. geol. Soc. Am.* **83**, 935–956.

Lister, G. S. 1978. Texture transitions in plastically deformed calcite rocks. In: *Proc. Conf. on Textures of Materials, Vol. II, Aachen* (edited by Gottstein, G. & Lücke, K.), 199–210.

Olgaard, D. L. & Evans, B. 1986. Effect of second-phase particles on grain-growth in calcite. *J. Am. Ceram. Soc.* **69**, c272–c272.

Owens, W. H. & Rutter, E. H. 1978. The development of magnetic susceptibility anisotropy through crystallographic preferred orientation in experimentally deformed marble. *Phys. Earth & Planet. Interiors* **16**, 215–222.

Padmanabhan, K. A. & Lücke, K. 1986. An assessment of the role of texture in structurally superplastic flow. *z. Metallkunde.* **77**, 765–770.

Rowe, K. J. & Rutter, E. H. 1990. Paleostress estimation using calcite twinning: experimental calibration and application to nature. *J. Struct. Geol.* **12**, 1–17.

Rutter, E. H. 1972. The influence of interstitial water on the rheological behaviour of calcite rocks. *Tectonophysics* **14**, 13–33.

Rutter, E. H. 1974. The influence of temperature, strain rate and interstitial water in the experimental deformation of calcite rocks. *Tectonophysics* **22**, 311–334.

Rutter, E. H. 1984. The kinetics of grain coarsening in calcite rocks. *Prog. Exp. Petrol.* **D25**, 245–249.

Rutter, E. H., Peach, C. J., White, S. H. & Johnson, D. 1985. Experimental 'syntectonic' hydration of basalt. *J. Struct. Geol.* **7**, 251–266.

Schmid, S. M., Boland, J. N. & Paterson, M. S. 1977. Superplastic flow in fine-grained limestone. *Tectonophysics* **43**, 257–291.

Schmid, S. M., Casey, M. & Starkey, J. 1981. The Microfabric of Calcite Tectonites from the Helvetic Nappes (Swiss Alps). *Spec. Publs geol. Soc. Lond.* **9**, 151–158.

Schmid, S. M., Pannozzo, R. & Bauer, S. 1987. Simple shear experiments on calcite rocks: rheology and microfabric. *J. Struct. Geol.* **9**, 747–778.

Spiers, C.J. 1979. Fabric development in calcite polycrystals deformed at 400°C. *Bull. Minéral.* **102**, 282–289.

Tough, J. G. 1988. The computation of the area, centroid and principal axes of a polygon. *Comput. & Geosci.* **14**, 715–717.

Tough, J. G. & Miles, 1984. A method for characterizing polygons in terms of the principal axes. *Comput. & Geosci.* **10**, 347–350.

Tullis, J. & Yund, R. A. 1985. Dynamic recrystallization of feldspar: a mechanism for ductile shear zone formation. *Geology* **13**, 238–241.

Walker, A. N., Rutter, E. H. & Brodie, K. H. 1990. Experimental study of grain-size sensitive flow of synthetic, hot-pressed calcite rocks. In: *Deformation Mechanisms, Rheology and Tectonics* (edited by Knipe, R. and Rutter, E.). *Spec. Publs geol. Soc. Lond.* **54**, 259–284.

Wenk, H. R., Venkitsubramanyan, C. W., Baker, D. W. & Turner, F. J. 1973. Preferred orientation in experimentally deformed limestone. *Contr. Miner. Petrol.* **38**, 81–114.

White, S. H. 1976. The effects of strain on the microstructure, fabrics and deformation mechanisms in quartzites. *Phil Trans. R. Soc. Lond.* **A283**, 69–86.